Effect of mean void fraction correlations on a shell-and-tube evaporator dynamic model performance

Joaquín Navarro Esbrí[1], Víctor Milián[2], Adrián Mota-Babiloni[1,2], Francisco Molés[1], Gumersindo Verdú[2]

[1]ISTENER Research Group, Department of Mechanical Engineering and Construction, University Jaume I, E12071 Castellón, Spain

[2]Institute for Industrial, Radiophysical and Environmental Safety, Camino de Vera s/n, Polytechnic University of Valencia, E46022 Valencia, Spain

Abstract

In this paper, the influence of different mean void fraction correlations on a shell-and-tube evaporator dynamic model performance has been evaluated. The model proposed is based on the moving boundary approach and includes the expansion valve modelling. Several transient tests, using R134a as working fluid, have been carried out varying refrigerant mass flow, inlet enthalpy and secondary fluid flow. Then, the model performance, using different mean void fractions, is analysed from the system model outputs (evaporating pressure, refrigerant outlet temperature and condensing water outlet temperature). The slip ratio expressions selected are: homogenous, momentum flux model, Zivi's, Chisholm's and Smith's correlations. The results of the comparison between experimental and model predictions depend on the transient characteristics and there is not a single slip ratio correlation that provides the best performance in all the cases analysed.

Keywords: evaporator; dynamic model; mean void fraction; slip ratio; refrigeration

Nomenclature

A	area (m^2)
A_K	expansion valve parameter (m^2)
B_K	expansion valve parameter (m^2 K^{-1})
c_p	specific heat capacity, (J kg^{-1} K^{-1})
D	diameter (m)
f	friction coefficient
F	Chen's forced convection correction factor
h	specific enthalpy (J kg^{-1})
k	thermal conductivity (W m^{-1} K^{-1})
k_A	expansion valve parameter (m^2)
L	evaporator zone length (m)
m	mass (kg)
$\dot{m}$	refrigerant mass flow rate (kg s^{-1})
n	summation upper bound
N	compressor speed (rpm)
P	pressure (Pa)
Pr	Prandtl number
Re	Reynolds number
S	Slip ratio
sf	Chen's suppression factor
$\dot{Q}$	cooling power (W)
T	temperature (K)
t	time (s)

u	dynamic viscosity (μPa s)
$\dot{V}$	volumetric flow rate ($m^3\ s^{-1}$)
x	vapour quality
X_{tt}	Martinelli parameter

Greek symbols

α	heat transfer coefficient ($W\ m^{-2}\ K^{-1}$)
γ	mean void fraction
ΔT	degree of superheating (K)
ΔT_{static}	static degree of superheating (K)
μ	density ratio
ρ	density (kg/m^3)
σ	vapour-liquid surface tension ($N\ m^{-1}$)
υ	specific volume ($m^3\ kg^{-1}$)

Subscripts

$actual$	experimental value
bf	two-phase
c	condensing
cat	catalogue
Ch	Chisholm's correlation
$conv$	convective

cs	cross section
e	evaporator
ex	external
g	glycol-water mixture
h	homogenous model
i	inlet
in	internal
k	*k*-value of a data set
L	saturated liquid
LV	liquid to vapour
M	metal surface
max	maximum
min	minimum
MF	momentum flux model
nb	nucleate boiling
r	refrigerant
s	shell
Sm	Smith's correlation
t	tube
Te	total evaporator length
o	outlet
V	saturated vapour
VS	vapour to superheating
Z	Zibi's correlation

1e	evaporation zone
2e	superheating zone

Acronyms

FV	finite-volume distributed-parameter model
MB	moving-boundary model
MVF	mean void fraction
RMS	Root mean square value

1. Introduction

Refrigeration facilities based on vapour compression cycles are responsible for about 30% of the total energy consumption (Bouzelin et al., 2005) for utility companies. Therefore, it is desirable to use appropriate models to improve both their performance and management. Most of the models used, either steady state or dynamic, are based on physical laws and they usually use fluid properties and components characteristics as input data.

When the aim of the model is simply to simulate specific conditions or to design systems and components, the steady state modelling is enough. In the available literature there are a lot of works that refer to steady state models of vapour compression systems (Gordon and NG, 2000), applied to different type of installations, as reciprocating (Bourdouxhe et al., 1994) or centrifugal (Braun et al., 1996) chillers. Browne and Bansal (1998) also reported different models of vapour-compression liquid chillers developed in the past decades and Li et al. (2014) reviewed the research advancement in dynamic modeling of HVAC equipment.

As vapour compression systems work most of the time under transient conditions (Roetzel and Xuan, 1999), steady state models cannot accurately describe the system response due to variations in their operating variables. Therefore, sometimes it is necessary to characterize the system transient behaviour by means of dynamic models. In this way, the characteristics of the systems can be better analysed, the new components can be properly designed and, finally, that could lead to improve its operation and efficiency. Bendapudi and Braun (2002) summarized various methodologies adopted in transient modelling and their applicability to chillers.

It is well-known that heat exchangers, and the types of changes related to their dynamics (Rasmussen and Shenoy, 2012), are the most complex parts of the vapour compression models. To describe the dynamic behaviour of heat exchangers three main approaches are commonly used (Rasmussen, 2012): finite-volume distributed-parameter (FV), moving-boundary lumped-parameter (MB) models and a hybrid technique of both. The general methodology applied in these approaches consists of applying the conservation equations into the heat exchanger control volumes.

On the one hand, when using the MB model, each control volume corresponds to those of the different fluid phase regions. In refrigeration and air conditioning evaporators, two zones are considered: evaporation zone and vapour superheating zone. The limits of those regions are the moving boundaries that determine their lengths, which in turn are dynamic variables. On the other hand, when using the FV model, the heat exchanger is divided in control volumes of a constant size.

Although FV models can be more accurate (MacArthur and Grald, 1989, Cullimore and Hendriks, 2001, Eborn et al., 2005 and Limperich et al., 2005) than MB models, they can require up to 15 control volumes to obtain good results (Bendapudi et al., 2008). This occurs because there are much more conservation equations than in the MB approach, resulting in a lower execution speed. MB models can be developed about three times faster than FV models and that is very important for control and diagnostic purposes (Bendapudi et al., 2008, Bendapudi, 2004).

The MB model was first pioneered by Wedekind et al. (1978). This approach uses the concept of a mean void fraction (MVF), calculated from the local void fraction and defined as the cross-sectional area occupied by the vapour in relation to the total area of the flow channel. This parameter can be calculated through different correlations and geometric definitions: local, chordal, volumetric and cross-sectional (commonly used for two-phase flow) (Collier and Thome, 1994 and Thome, 2004).

Extensive lists of void fraction models and correlations for internal flow are given by Rice (1987), Woldesemayat and Ghajar (2007), and Dalkilic *et al.* (2008). Among them, one of the most common are the slip ratio correlations, where the void fraction depends on the vapour quality and some fluid properties (Wallis, 1969). Dalkilic *et al.* (2008) realized a comparison in a vertical smooth tube (in steady state flow) and concluded that most of the slip ratio correlations have results that are compatible with each other for the same operating conditions. Milian *et al.* (2013) developed a dynamic model of a shell-and-tube condenser and studied their performance using different mean void fraction correlations. In the dynamic model (using R407C) of Haberschill et al., (2003) was simulated the control of cooling capacity by opening the expansion valve and by varying the compressor speed.

The aim of this paper is to develop of a MB dynamic model of a Direct Expansion evaporator (including the expansion valve model) evaluating the influence of different slip ratio correlations on the model performance. The evaluation is quantified comparing the model predictions and the experimental data measurements for different transient situations in a vapour compression system using R134a as refrigerant.

The rest of the paper is organized as follows. In Section 2, the proposed model is described. In Section 3, the correlations used to obtain the different mean void fractions are presented. In Section 4, the experimental test bench and tests used to validate the model are briefly explained. In section 5 the results are showed and, finally, in section 6 the main conclusions of this work are summarized.

2. Model description

An overview of the structure of the proposed model is shown in Fig. 1.

Fig. 1. Model scheme.

The model takes five parameters as input variables: refrigerant mass flow rate, $\dot{m}_r$, evaporator inlet refrigerant enthalpy, h_{ie}, propylene glycol-water mixture mass flow rate and temperature, $\dot{m}_g$ and $T_{g,ie}$, respectively, and expansion valve static superheating degree, ΔT.

The model outputs are: length of evaporating zone, L_{1e}, evaporating pressure, P_e, evaporator outlet refrigerant enthalpy, h_{oe}, and tube wall temperatures in evaporation zone (*1e*) and superheating zone (*2e*), $T_{t,1e}$ and $T_{t,2e}$, respectively. From these outputs it can be easily derived the other measurable outputs, refrigerant outlet temperature, $T_{r,oe}$, and glycol-water outlet temperature, $T_{g,oe}$.

The expansion valve and evaporator model equations, the mean void fractions expressions used and the applied heat transfer coefficients are presented below.

2.1. Expansion valve

According to previous studies (Rasmussen, 2005), the expansion valve mechanical dynamics are significantly faster than the expansion valve thermal dynamics, being the latter similar to the vapour compression system dynamics. Due to this difference, the valve is modelled with static relationships.

Under normal operation the mass flow rate through the component is a fraction of the maximum value given by the manufacturer's catalogue and is given by Eq. (1) (Belman et al., 2010).

$$\dot{m}_r = \dot{m}_{r,cat} \frac{\Delta T_{static} - \Delta T}{\Delta T_{static,max} - \Delta T} \quad (1)$$

$\dot{m}_{r,cat}$ is given in the Eq. (2).

$$\dot{m}_{r,cat} = k_A\sqrt{\rho_L(P_c - P_e)} \quad (2)$$

k_A is a parameter characterized by a general correlation (Saiz Jabardo et al., 2002) presented in Eq. (3).

$$k_A = A_k + B_k\, T_e \quad (3)$$

A_k and B_k depend on the valve chosen. For the current valve are equal to $2.433 \cdot 10^{-6}$ m^2 and $4.857 \cdot 10^{-8}$ $m^2\ K^{-1}$ (Belman et al., 2010).

The initial value of static superheating degree is obtained from manufacturer's data. Besides, an experimental correlation for the maximum superheating degree in terms of the static superheating degree is given by Eq. (4) (Belman et al., 2010).

$$\Delta T_{static,max} = -0.75 + 1.75\Delta T \quad (4)$$

º

2.2. Evaporator

For modelling purposes, the refrigerant flow in the shell-and-tube evaporator (Fig. 2a) can be approached to an equivalent axial tube heat exchanger (Fig. 2b) (Grald and MacArthur, 1992). Thus, it can be considered that the glycol water mixture flows through the outer tube and the inner tube carries the refrigerant.

Fig. 2. Shell-and-tube evaporator inner structure and fluid path (a), and equivalent axial tube with two evaporator zones (b).

As can be seen in Fig. 2, the evaporator is represented with two zones: evaporation zone and superheating zone, whose lengths are the model outputs L_{1e} (being also the moving boundary) and L_{2e}, respectively.

In what follows, the governing partial differential equations are described, as well as the way to obtain the governing ordinary differential equations of the lumped parameter model.

The main simplifying assumptions of the model are as follow:

- The mass flow rate of the refrigerant is assumed to be the same throughout the two components of the subsystem.
- The fluid flow in the evaporator is one-dimensional.
- Pressure drops are negligible.
- The expansion process through the thermostatic expansion valve is isenthalpic.
- There is no axial heat transfer conduction in the fluid flow.
- There is no axial heat transfer conduction in the tube wall, and there is no wall temperature variation along its cross section.
- Heat conduction through the shell can be neglected.

The evaporator zones can be modelled from the Navier-Stokes generalized equations (Willatzen et al., 1998) and from the energy conservation equation in the evaporator's wall.

Due to the simplifying assumptions, the momentum equation can be eliminated (Eq. (5), (6) and (7)).

$$\frac{\partial \rho A_{cs}}{\partial t} + \frac{\partial \dot{m}_r}{\partial z} = 0 \qquad \text{Refrigerant mass balance} \qquad (5)$$

$$\frac{\partial (\rho A_{cs} h - A_{cs} P_e)}{\partial t} + \frac{\partial (\dot{m}_r h)}{\partial z} = \alpha_{in} \pi D_{in} (T_t - T_r) \qquad \text{Refrigerant energy balance} \qquad (6)$$

$$m_{te} c_{p,t} \frac{\partial T_t}{\partial t} = \alpha_{in} \pi D_{in} L (T_r - T_t) + \alpha_{ex} \pi D_{ex} L \left(T_g - T_t\right) \qquad \text{Tube wall energy balance} \qquad (7)$$

The spatial dependence of the previous partial differential equations is taken away by integrating the equations over the length of each region (Zhang et al., 2006). By applying Leibnitz's rule on the first terms and integrating the second terms, a set of six ordinary differential equations is obtained. The integration of Eq. (5) and (6) in the two-phase flow region requires to use the concept of mean void fraction, γ, to characterize the density and enthalpy, Eq. (8) and (9).

$$\rho = \rho_L (1 - \gamma) + \rho_V \gamma \qquad (8)$$

$$\rho h = \rho_L h_L (1 - \gamma) + \rho_V h_V \gamma \qquad (9)$$

The six aforementioned ordinary differential equations are reduced to five after removing the refrigerant flow rate at the intermediate point, $\dot{m}_{int}$, where vapour quality is 1. The resulting

equations are shown in a compact form in Eq. (10) and the equations terms z_{ij} and y_{ij} are given in Table 1 and Table 2.

$$\begin{bmatrix} z_{11} & z_{12} & 0 & 0 & 0 \\ z_{21} & z_{22} & z_{23} & 0 & 0 \\ z_{31} & z_{32} & z_{33} & 0 & 0 \\ 0 & 0 & 0 & z_{44} & 0 \\ z_{51} & 0 & 0 & 0 & z_{55} \end{bmatrix} \begin{bmatrix} \dot{L}_{1e} \\ \dot{P}_e \\ \dot{h}_o \\ \dot{T}_{t,1e} \\ \dot{T}_{t,2e} \end{bmatrix} = \begin{bmatrix} y_{11} + \rho_L(h_L - h_V)A_{cs,e}\dot{\gamma}L_{1e} \\ y_{12} - (\rho_V - \rho_L)h_V A_{cs,e}\dot{\gamma}L_{1e} \\ y_{13} - (\rho_V - \rho_L)A_{cs,e}\dot{\gamma}L_{1e} \\ y_{14} \\ y_{15} \end{bmatrix} \quad (10)$$

Table 1. Terms z_{ij} in system model.

Table 2. Terms y_{ij} in system model.

In this model, the enthalpy in the superheating zone, h_{2e}, has been taken as the mean value between input and output enthalpy values of the zone. Then, all the other refrigerant properties are calculated from the pressure and mean enthalpy obtained in each iteration step. Refrigerant properties as well as their time derivatives have been obtained from fitting equations derived from the values provided by REFPROP library (Lemmon et al., 2002), what reduces the execution time in about three times.

2.3. Heat transfer coefficients

To obtain the heat transfer coefficients, α, there are many expressions available in the open literature (Bendapudi and Braun, 2002) for each different heat exchanger geometric configurations. In this case, as the model is intended to be used in both steady state and dynamic situations, it has been chosen those expressions which have shown a good performance in previous works such as entire vapour compression models (Navarro-Esbrí et al., 2010) or shell-and-tube evaporator models (Navarro-Esbrí et al., 2014). The correlations selected and the equations used are expressed in Table 3.

Table 3. Equations used to obtain the heat transfer coefficients.

2.4. Mean void fraction correlations

The mean void fraction and its time derivative are included in the z_{ij} coefficients (coefficient matrix) of the previous model, Eq. (10). Although there are different correlations for predicting void fraction in refrigeration applications (Wilson et al., 1998), in this work it is chosen the local slip ratio (which can be correlated with different void fraction expressions). The equation to calculate this parameter is shown in Eq. (11).

$$\gamma_{local} = \frac{x}{x + (1-x)\mu S} \tag{11}$$

where $\mu = (\rho_V / \rho_L)$ and S is the slip ratio (or velocity ratio), which is defined as the ratio between the vapour and liquid speeds in the two-phase region (Thome, 2004).

If S=1 is selected, the homogeneous model is obtained (S_h). However, some authors note that it can be an inadequate representation and propose a slip flow two-phase model with S>1 because it provides improved experimental results (Jakobsen et al., 1999).

The analytical void fraction models assume that some quantities, such as momentum or kinetic energy of the two phases, tend towards a minimum value. So, when the momentum flux is assumed to have a minimum value (S_{MF}) the velocity ratio S is given by Eq. (12).

$$S_{MF} = \left(\frac{\rho_V}{\rho_L}\right)^{-1/2} \tag{12}$$

Another frequently used expression to calculate S is proposed by Zivi (S_Z) (Rice, 1987), Eq. (13). This model was proposed for annular flow, with the assumption that no liquid is entrained in the central vapour core and that the total kinetic energy of the two phases will tend to be a minimum.

$$S_Z = \left(\frac{\rho_V}{\rho_L}\right)^{-1/3} \tag{13}$$

Aside from the previous analytical models, two empirical correlations obtained by Smith and Chisholm are also used in this model (Collier and Thome, 1994). These correlations depend on both evaporating pressure and vapour quality.

The Smith separated flow model provides the following slip ratio expression (S_{Sm}), Eq. (14).

$$S_{Sm} = e + (1-e)\left[\frac{\frac{\rho_L}{\rho_V} + e\left(\frac{1-x}{x}\right)}{1 + e\left(\frac{1-x}{x}\right)}\right]^{1/2} \tag{14}$$

where *e* represents the fraction of liquid entrained in the gas as droplets. Eq. (14) is based on the assumption that the momentum fluxes in both phases are equal (Rice, 1987).

The Chisholm correlation (S_{Ch}) is derived from simple annular flow theory and equates the frictional pressure drops in the liquid and the gas phase, Eq. (15).

$$S_{Ch} = \left[1 - x\left(1 - \frac{\rho_L}{\rho_V}\right)\right]^{1/2} \tag{15}$$

So, in this paper, five slip ratio correlations are used: S_h, S_{MF}, S_Z, S_{Sm}, S_{Ch}. These expressions can be used in Eq. (11) to obtain the mean void fraction.

In this way, after using S_{MF} or S_Z in Eq. (11) and integrating along the two-phase zone, it can be obtained the mean void fraction, $\gamma(x, S)$, Eq. (16). This expression depends on both the vapour quality and on the slip ratio correlation used (Fig. 3 represents the mean void fraction values obtained when $S = S_Z$, varying μ and the vapour inlet quality).

$$\gamma = \frac{1}{(1-\mu S)}\left\{1 + \frac{\mu S}{(x_{2e} - x_{1e})(1-\mu S)}\, ln\left[\frac{\mu S + x_{1e}(1-\mu S)}{\mu S + x_{2e}(1-\mu S)}\right]\right\} \tag{16}$$

Fig. 3. Quality based mean void fraction, S=S_Z.

However, when substituting S_{Sm} or S_{Ch} in Eq. (11), the resulting expression cannot be solved analytically. Instead, a numerical integration can be performed as proposed in Eq. (17). n is the total amount of nodes, in this case it is equal to 10 in order to have enough accuracy (Zhang and Zhang, 2006).

$$\gamma = \frac{1}{n}\sum_{k=1}^{n}(\gamma_{local})_k \tag{17}$$

The time derivative $\dot{\gamma}$ (included in the right hand terms of the Eq. (10)) can be neglected in this case. This is because the mean void fractions calculated take almost constant values (this can be seen for $S = S_Z$ in Fig. 3, particularly for μ<0.01).

The slip ratios S_{MF} and S_Z only depend on the evaporating pressure, and are calculated straightforward at each program step. But as S_{Sm} and S_{Ch} also depend on the vapour quality at each point of the evaporating zone, their mean values must be calculated at each time step along this zone; this is performed approximately by means of numeric integration.

3. Experimental plant and tests

The experimental plant is composed of a vapour compression system, using R134a as working fluid, and two secondary fluid circuits (Fig. 4). The main circuit consists of an open type variable speed compressor, a shell-and-tube condenser, with refrigerant flowing along the shell and the water inside the tubes; a thermostatic expansion valve, and a DX shell-and-

tube evaporator thermally isolated, where the refrigerant flows inside the tubes (Table 4) and the secondary fluid along the shell.

Fig. 4. Simplified vapour compression plant scheme.

Table 4. Tube characteristics.

The evaporator secondary fluid circuit is a load simulation system (it makes possible to control the evaporator conditions). It consists of a tank with electrical resistances allowing the control of the evaporator's thermal load by means of a variable speed pump and a PID temperature controller. The secondary fluid is a water–propylene glycol (70/30 by mass percentage).

The experimental setup is fully instrumented to measure key variables (their location can be seen at Fig 4.) Table 5 shows a summary of the measured parameters, the sensors used and the uncertainty associated. The signals generated are gathered with a data acquisition system and monitored and controlled through a personal computer.

Table 5. Measured parameters and equipment uncertainty.

In order to carry out a proper model validation, the transient tests were realised over a wide range of operating conditions (Table 6). In each transient test, only one input changes: mass flow rate, evaporator inlet enthalpy or glycol-water mixture flow rate. First, these parameters are lowered (or increased) and subsequently are increased (or lowered) in about the same amount. The static superheating degree is maintained constant at 5K, and the rest of the inputs remain almost stable (their mean values and standard deviation are also shown).

Table 6. Parameters changes that originates the transients.

4. Results and discussion

In this section the comparison between experimental and model predictions using different slip ratio correlations (mentioned in brackets for each parameter considered) is presented. Thus, the predicted model outputs (evaporating pressure, refrigerant outlet temperature and glycol-water outlet temperature), using different slip ratios correlations, are compared with the experimental measurements (Fig. 5 to Fig. 10). It is also shown how the MVF corresponding to those slip ratios behave over the course of the tests.

As said before, the model inputs are incremented and decremented in the same amount. But since the trends are similar, it is only shown the model outputs for one performed change (either decrease or increase).

The root mean square (RMS) deviation is used to quantify the difference between each value predicted by the model X_S and the experimental value measured X_{actual}, Eq. (18).

$$RMS(X) = \sqrt{\frac{\sum_{k=1}^{n}\left(X_{actual,k} - X_{S,k}\right)^2}{n}} \tag{18}$$

X represents the outputs $P_e, T_{r,oe}, T_{g,oe}$ and the subindex S represents the slip ratio expression used, described above (S=*h, MF, Z, Sm, Ch*). *k* is the *k*-value of the data set and model results and n represents the total amount of measurements in each test. The RMS values obtained with each void fraction correlation are given in Table 7.

Table 7. RMS values.

In the following paragraphs, the system responses due to changes in input variables (refrigerant mass flow rate, evaporator inlet quality or glycol-water mixture flow rate) are analysed.

4.1. Changes in refrigerant mass flow rate

The changes in refrigerant mass flow rates are contemplated in tests from 1 to 6, with small changes (test 1 and test 2), medium changes (test 3 and test 4) and high changes (test 5 and test 6).

As shown in Table 6, the refrigerant mass flow rate in test 1 is changed from 0.0563 to 0.0548 $kg\ s^{-1}$, and in test 2 it has been changed from 0.0555 to 0.0569 $kg\ s^{-1}$. Both variations can be considered as small changes. The transient responses of the system model outputs for test 1 are shown in Fig. 5.

Fig. 5. Test 1. Model outputs due to small decrease in refrigerant mass flux, (a) evaporating pressure, (b) refrigerant outlet temperature, (c) secondary fluid outlet temperature.

As can be seen in Fig. 5, the model correctly predicts the dynamics of the three outputs. The model results are very similar for P_e and $T_{r,oe}$ (except with the homogeneous model) and converge quite well to the experimental values (being particularly good for $T_{g,oe}$), although a slight slower response in pressure predictions is detected. As the trend and dynamics of all outputs in test 2 are similar to those in test 1, the test 2 graphics are not shown in this paper.

From the RMS values given in Table 7, it can be deduced that the slip ratio that produces best model performance, in terms of RMS values, in both tests is S_{MF} for P_e and $T_{r,oe}$ (except in Test 2, where S_Z is a slight better), being the model predictions obtained using S_{Ch}, S_{Sm} and S_Z very close. The slip ratio that produces the highest values of RMS in the evaporating pressure and refrigerant outlet temperature is the homogeneous model.

From Table 7 it can also be seen that for $T_{g,oe}$, the RMS differences are almost negligible.

The next group of transient responses are obtained with medium changes in refrigerant mass flow. Test 3 when it drops from 0.0556 to 0.0503 $kg\ s^{-1}$ and test 4 when it increases in about the same quantity from 0.0483 to 0.0543 $kg\ s^{-1}$. In these two tests the changes are higher than previously. The model outputs transients for test 3 are shown in Fig. 6.

Fig. 6. Test 3. Model outputs due to medium decrease in refrigerant mass flux, (a) evaporating pressure, (b) refrigerant outlet temperature, (c) secondary fluid outlet temperature.

From Fig. 6 it can be seen that the model predicts correctly enough the dynamics of the three outputs, being the homogeneous correlation the one that gives higher errors in model predictions. The output trends are similar in both tests 3 and 4. All RMS values in tests 3 and 4 are greater than in tests 1 and 2.

According to the RMS values, the best performing slip ratios, in terms of RMS values, for P_e and $T_{r,oe}$in both tests are S_{Ch} and S_{Sm} (and their results are very similar). Equal to tests 1 and 2, the worst values are given by S_h.

Fig. 6c shows that $T_{g,oe}$ follows and approaches very well to the experimental values for all correlations. The maximum relative error in both tests is 0.13% for $T_{g,oe}(S_{Ch})$.

In test 5 and 6 the highest changes in mass flow rate are performed: in test 5 it drops from 0.0569 $kg\ s^{-1}$ to 0.0497 $kg\ s^{-1}$ and in test 6 it increases in a similar quantity, from 0.0497 $kg\ s^{-1}$ to 0.0603 $kg\ s^{-1}$. Fig. 7 shows the behavior of the three model outputs in test 5. The

transients of these model outputs also follow the experimental trends, particularly $T_{g,oe}$. The other two outputs, i.e., P_e and $T_{r,oe}$, depart from the experimental values even more than in previous tests. RMS results for each slip ratio correlation are now even higher than in previous tests.

Fig. 7. Test 5. Model outputs due to high decrease in refrigerant mass flux, (a) evaporating pressure, (b) refrigerant outlet temperature, (c) secondary fluid outlet temperature.

For these two tests, the RMS results for P_e and $T_{r,oe}$ are very similar to the previous tests. The empirical correlations of Smith and Chisholm are the best performing and, again, the worst performing correlation is S_h.

As in previous tests, the model using any of the proposed slip ratio correlations follows and approaches very well to the experimental values for all correlations.

4.2. Changes in evaporator inlet enthalpy

The changes in evaporator inlet enthalpy are represented by tests from 7 to 10. Test 7 and test 8 show small changes and test 9 and test 10 present higher changes.

Analysing the small changes, in test 7 (Fig. 8), evaporator inlet enthalpy increases from about 251 to 258 $kJ\ kg^{-1}$, whereas in test 8, the inlet enthalpy drops from 256 to 251 $kJ\ kg^{-1}$.

Fig. 8. Test 7. Model outputs due to small decrease in evaporator inlet enthalpy, (a) evaporating pressure, (b) refrigerant outlet temperature, (c) secondary fluid outlet temperature.

Using all the slip ration correlations (except the homogenous one), the model outputs follow quite well the experimental values. As in all cases seen up till now, the homogeneous model predicts a lower pressure and a higher temperature than the experimental values, so both departs significantly.

The model predictions using S_{Ch}, S_{Sm} and S_Z are very next to the actual values for P_e and $T_{r,oe}$. Even S_Z is giving good model predictions. About $T_{g,oe}$ model predictions, again all the MVF correlations provide good results as it can be seen also in Fig 8.c.

Regarding to higher changes in evaporator inlet enthalpy, represented by test 9 and test 10, Fig. 9 shows the results of test 9. It can be seen as the results with the homogeneous correlation depart significantly from the other (as in previous tests). Comparing these results with those obtained in the previous test which evaporator inlet enthalpy is varied (7 and 8), it can be seen as the model outputs are closer to experimental values when inlet enthalpy variations are small. Besides, predictions are better when inlet enthalpy decreases. This can be stated analysing the RMS values.

Fig. 9. Test 9. Model outputs due to high decrease in evaporator inlet enthalpy, (a) evaporating pressure, (b) refrigerant outlet temperature, (c) secondary fluid outlet temperature.

According to the RMS values obtained for P_e in both tests 9 and 10, the best performing slip ratio is given by the homogeneous correlation. The maximum relative errors are observed in $P_e(\mathrm{S_{Ch}})$ and are: 3.30% and 2.37% in tests 9 and 10, respectively. RMS values in test 9 are higher than in test 7 and RMS values in test 10 are higher than in test 8. Thus, as it happens in the case of refrigerant mass flux changes, enthalpy variations also affect model deviations from the experimental values.

For $T_{r,oe}$, as well as in tests 7 and 8, the homogeneous correlation is the worst performing with relative errors of 0.46% and 0.22% for $T_{r,oe}(S_{Ch})$ in test 9 and 10. For $T_{g,oe}$, maximum relative errors are less than 0.1% for $T_{g,oe}(S_Z)$ in both tests 9 and 10.

4.3. Changes in glycol-water mixture flow

The next set of transient tests is the result of changes in propylene glycol water mixture flow (tests 11 and 12). In Fig. 10 the model outputs of test 11 are represented, which corresponds to a sharp glycol-water flow increase of 2.3 10^{-4} m^3 s^{-1}, (in test 12 a similar drop in glycol-water flow takes place). Once more the model outputs trends follow quite well the experimental values, and results with the homogeneous model depart significantly from the others, the latter being quite similar to each other.

Fig. 10. Test 11. Model outputs due to sharp decrease in evaporator secondary fluid flow, (a) evaporating pressure, (b) refrigerant outlet temperature, (c) secondary fluid outlet temperature.

The model predictions for P_e and $T_{r,oe}$ in tests 11 and 12 are worst that those obtained in all the previous tests, being the RMS values very similar for all the slip ratio correlations. The homogeneous model continues producing a model overestimation in refrigerant outlet temperature and an underestimation in evaporating pressure in comparison to the other MVF correlations.

Again, $T_{g,oe}$ is predicted accurately using any of the correlations proposed in this work.

5. Conclusions

This paper presents a dynamic lumped parameter model for an evaporator with thermostatic expansion valve, using R134a as working fluid. The heat exchanger is modelled with the moving-boundary formulation whereas the expansion valve is described by a steady state model. In this model, several slip ratio correlations, used to calculate the mean void fraction parameter, have been used, and their influence on the model results has been analysed, comparing model predictions with experimental data measured from transient tests.

In general, the physical model used in this work predicts the evaporating pressure with a maximum relative error of ±8%, and the refrigerant and evaporator secondary fluid output temperatures with maximum relative errors always below 2%. As these errors usually

correspond to the worst performing slip ratios of each case, smaller errors are obtained with other slip ratio correlations.

The influence of the slip ratio correlations on the model accuracy depends on the output considered, the transient situation chosen. For refrigerant mass flow rate variations, in general, the most accurate model predictions are obtained when Chisholm's or Smith's correlations are used. For evaporator inlet enthalpy changes Chisholm's or Smith's produce good model predictions, and Zivi's correlation for high changes. For secondary fluid flow variations, the results provided by Chisholm's and Smith's correlations and by the momentum flux model are very similar.

References

Belman, J.M., Navarro-Esbrí, J., Ginestar, D. and V. Milián, 2010. Steady-state model of a variable speed vapour compression system using R134a as a working fluid. International Journal of Energy Research 34(11): 933-945.

Bendapudi, S. 2004. Development and evaluation of modeling approaches for transients in centrifugal chillers. PhD thesis, Purdue University.

Bendapudi, S. and J.E. Braun, 2002. A Review of Literature on Dynamic Models of vapour Compression Equipment, ASHRAE Report; No. 4036–5.

Bendapudi, S., Braun, J.E. and E.A. Groll, 2008. A comparison of moving-boundary and finite-volume formulations for transients in centrifugal chillers. International Journal of Refrigeration 31: 1437–1452.

Bourdouxhe, J.P., Grodent, M., Lebrun, J.J. and C.A. Saavedra, 1994. A toolkit for primary HVAC system energy calculation – part 2: reciprocating chiller models, ASHRAE Transactions 100: 774–786.

Bouzelin, L.O.S., Amico, S.C., Vargas, J.V.C. and J.A.R. Parise, 2005. Experimental development of an intelligent refrigeration system. International Journal of Refrigeration 28: 165–175.

Braun, J.E., Mitchell, J.W., Klein, S.A. and W.A. Beckman, 1996. Models for variable speed centrifugal chillers. System simulation in buildings, in: Proceedings of the International Conference in Liege, Belgium pp. 83–111.

Browne, M.W. and P.K. Bansal, 1998. Challenges in modeling vapour compression liquid chillers. ASRHAE Transactions 104 (Part 1A): 474–486.

Chen, J.C. 1966. A correlation for boiling heat transfer of saturated fluids in convective flow. Industrial and Engineering Chemistry Process Design and Development 5: 322–329.

Collier, J.G. and J.R. Thome, 1994. Convective Boiling and Condensation. Clarendon Press. Oxford.

Cullimore, B.A. and T.J. Hendricks, 2001. Design and transient simulation of vehicle air conditioning systems. SAE Paper 2001-01-1692.

Dalkilic, A.S., Laohalertdecha, S. and S. Wongwises, 2008. Effect of void fraction models on the two-phase friction factor of R134a during condensation in vertical downward flow in a smooth tube. International Communications in Heat and Mass Transfer 35: 921-927.

Dittus, F.W. and L.M.K. Boelter, 1930. Publications on Engineering, vol. 2. University of California: Berkeley.

Eborn, J., Tummescheit, H. and K. Prölß, 2005. Air conditioning – a modelica library for dynamic simulation of AC Systems. In: Proceedings of the Fourth International Modelica Conference, March 7–8, Hamburg-Harburg, Germany, 2005, pp: 185–192.

Forster, H.K. and N. Zuber, 1955. Dynamics of vapour bubble growth and boiling heat transfer. AIChE Journal 1955;1: 531–535.

Gado, A., Hwang. Y. and R. Radermacher, 2008. Dynamic Behavior of Mobile Air-Conditioning Systems. HVAC&R Research 14(2): 307-321.

Gnielinski, V. 1976. New equations for heat and mass transfer in turbulent pipe and channel flow. International Chemical Engineering 16: 359–368.

Gordon, J.M. and K.C. Ng, 2000. Cool Thermodynamics. International Science Publishing: Cambridge.

Grald, E.W. and J.W. MacArthur, 1992. A moving-boundary formulation for modeling time-dependent two-phase flows. International Journal of Heat and Fluid Flow 13(3): 266–272.

Haberschill, P., Gay, L., Aubouin, P. and M. Lallemand, 2003. Dynamic Model of a Vapor-Compression Refrigerating Machine Using R-407C. HVAC&R Research 9(4): 451-566.

Incropera, F.P. and D.P. DeWitt, 1996. Fundamentals of Heat and Mass Transfer, 4nt Edition, John Wiley&Sons.

Jakobsen, A., Antonius, J. and H.J. Hagaard-Knudsen, 1999. Experimental evaluation of the use of homogeneous and slip-flow two-phase dynamic models in evaporator modeling. In: Proceedings of the 20th International Congress of Refrigeration (Sydney) 1999. Paper no. 135.

Lemmon, E.W., Huber, M.L. and M.O. McLinden, 2007. REFPROP, NIST Standard Reference Database 23, v.8. National Institute of Standards, Gaithersburg, MD, USA.

Li, P., Qiao, H., Li ,Y., Seem J.E., Winkler J. and X. Li, 2014. Recent advances in dynamic modeling of HVAC equipment. Part 1: Equipment modelling. HVAC&R Research 20(1): 136-149.

Limperich, D., Braun, M., Schmitz, G. and K. Prölß, 2005. System simulation of automotive refrigeration cycles. In: Proceedings of the Fourth International Modelica Conference, March 7–8, Hamburg-Harburg, Germany 2005, pp: 193–199.

MacArthur, J.W. and E.W. Grald, 1989. Unsteady compressible two-phase flow model for predicting cyclic heat pump performance and a comparison with experimental data. International Journal of Refrigeration 12(1): 29–41.

Milián, V., Navarro-Esbrí, J., Ginestar, D., Molés, F. and B., Peris, 2013. Dynamic model of a shell-and-tube condenser. Analysis of the mean void fraction correlation influence on the model performance. Energy 59: 521-533.

Navarro-Esbrí, J., Ginestar, D., Belman, J.M., Milián, V. and G. Verdú, 2010. Application of a lumped model for predicting energy performance of a variable-speed vapour compression system. Applied Thermal Engineering 30(4): 286-294.

Navarro-Esbrí, J., Molés, F., Peris, B., Barragán-Cervera, A., Mendoza-Miranda, J.M., Mota-Babiloni, A. and J.M. Belman, 2014. Shell-and-tube evaporator model performance with different two-phase flow heat transfer correlations. Experimental analysis using R134a and R1234yf. Applied Thermal Engineering 62(1):80-89.

Rasmussen, B.P. 2005. Dynamic Modeling and Advanced Control of Air Conditioning and Refrigeration Systems, Dept. of Mechanical Engineering, University of Illinois.

Rasmussen, B.P. 2012. Dynamic modeling for vapor compression systems— I: Literature review. HVAC&R Research 18(5): 934-955.

Rasmussen, B.P. and B. Shenoy, 2012. Dynamic modeling for vapor compression systems—Part II: Simulation tutorial. HVAC&R Research 18(5): 956-973.

Rice, C.K. 1987. The effect of void fraction correlation and the heat flux assumption on refrigerant charge inventory predictions. ASHRAE Transactions 93(1) pp: 341-367.

Roetzel, W. and Y. Xuan, 1999. Dynamic Behaviour of Heat Exchangers, Vol.3. WITPress/Computational Mechanics Publications.

Saiz Jabardo, J.M., Gonzales Mamani, W. and M.R. Ianella, 2002. Modeling and experimental evaluation of an automotive air conditioning system with a variable capacity compressor. International Journal of Refrigeration 25: 1157–1172.

Thome, J.R. 2004. Wolverine Heat Transfer Engineering Data book III, Wolverine Tube Inc.

Wallis, G.B. 1969. One-dimensional two-phase flow. McGraw-Hill.

Wedekind, G.L., Bhatt, B.L. and B.T. Beck, 1978. A system mean void fraction model for predicting various transient phenomena associated with two phase evaporating and condensing flows. International Journal of Multiphase Flow 4: 97–114.

Willatzen, M., Pettit, N.B.O.L. and L. Ploug-Sørensen, 1998. A general dynamic simulation model for evaporators and condensers in refrigeration, Part I: moving-boundary formulation of two-phase flows with heat exchange. International Journal of Refrigeration 21: 398 – 414.

Wilson, M.J., Newell, T.A. and J.C. Chato, 1998. Experimental Investigation of Void Fraction during Horizontal Flow in Larger Diameter Refrigeration Applications, Air Conditioning and Refrigeration Center, University of Illinois at Urbana Champaign. ACRC TR-140.

Woldesemayat, M.A. and A.J. Ghajar, 2007. Comparison of void fraction correlations for different flow patterns in horizontal and upward inclined pipes. International Journal of Multiphase Flow 33: 347–370.

Zhang, W.J. and C.L. Zhang, 2006. A generalized moving boundary model for transient simulation of dry-expansion evaporators under larger disturbances. International Journal of Refrigeration 29: 1119–1127.

Zukauskas, A.A. 1987. Convective heat transfer in cross flow. In Handbook of Single-Phase Convective Heat Transfer, Kakac S, Shah RK, Aung W (eds). Wiley: New York, 6.1–6.45.

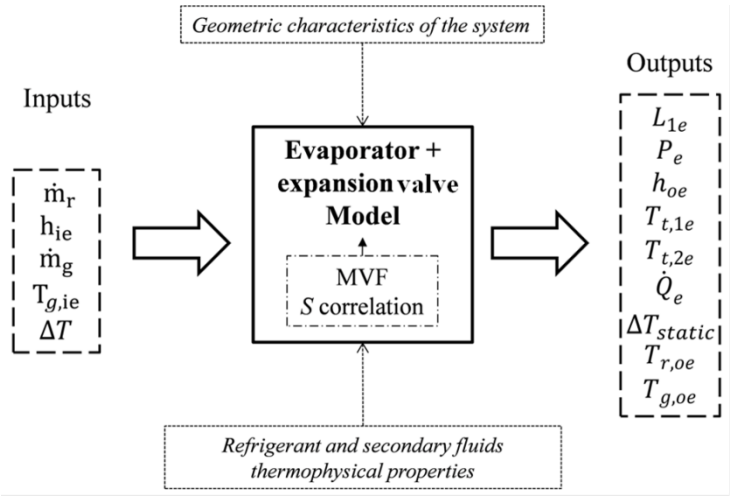

Fig. 1. Model scheme.

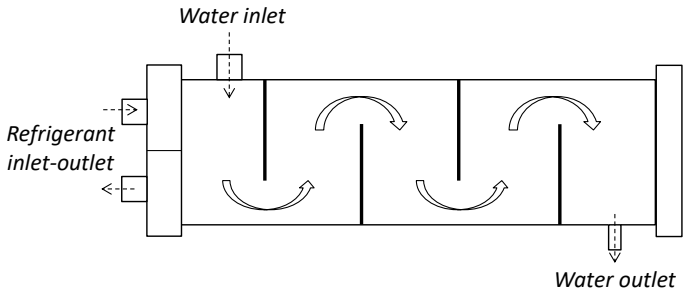

(a)

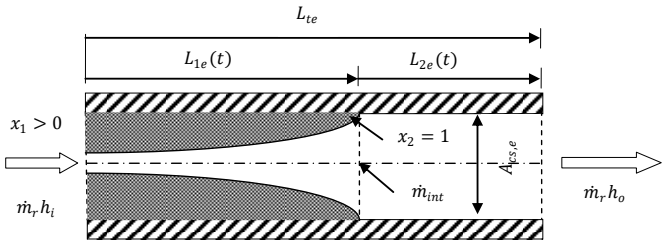

(b)

Fig. 2. Shell-and-tube evaporator inner structure and fluid path (a) and equivalent axial tube with two evaporator zones (b).

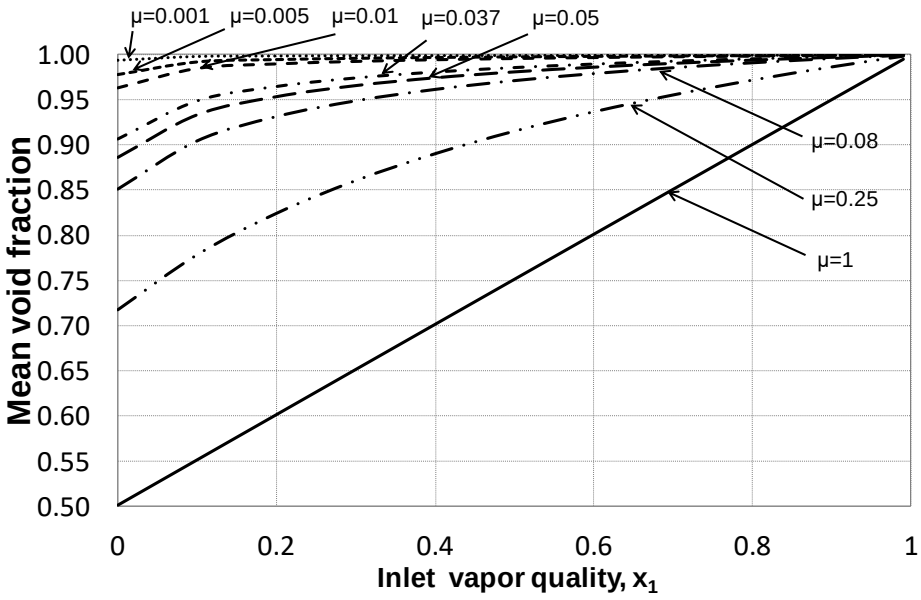

Fig. 3. Quality based mean void fraction, S=S_Z.

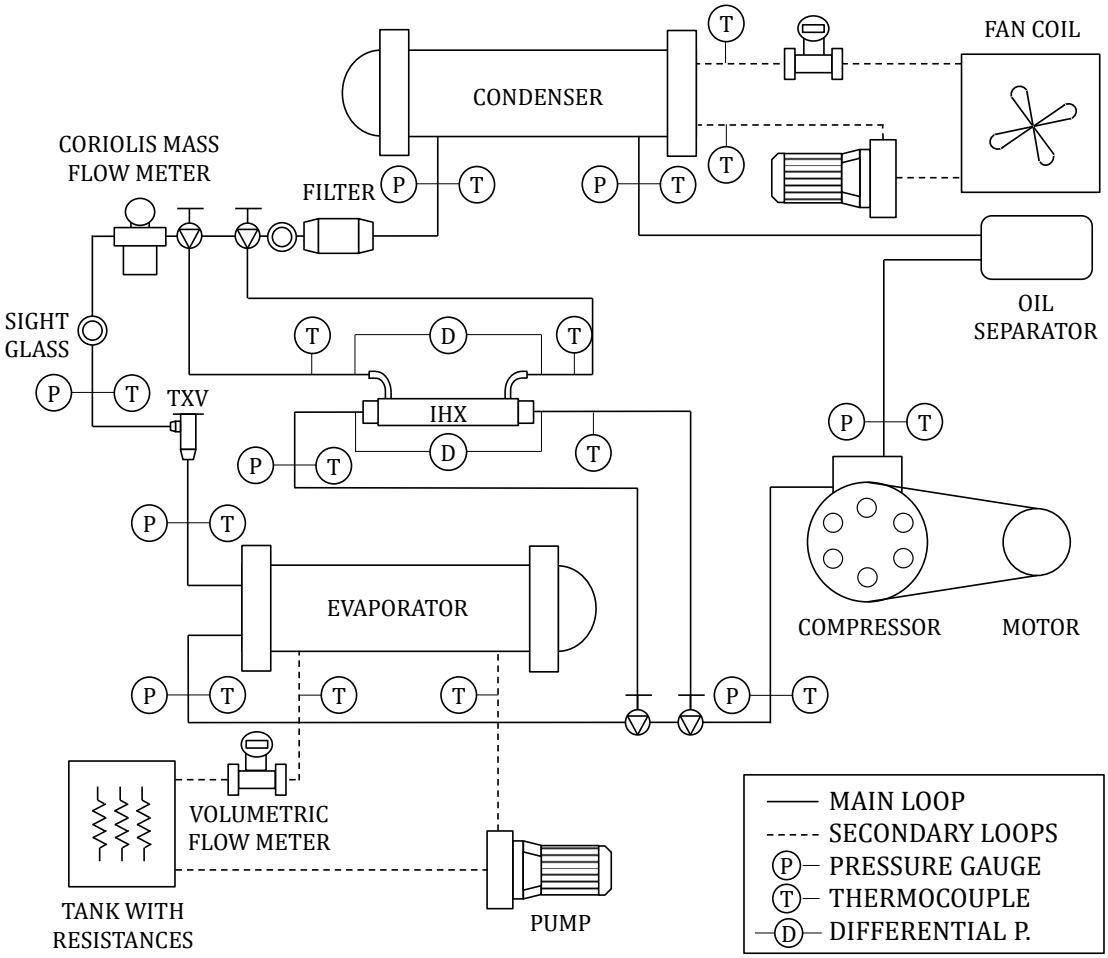

Fig. 4. Simplified vapour compression plant scheme.

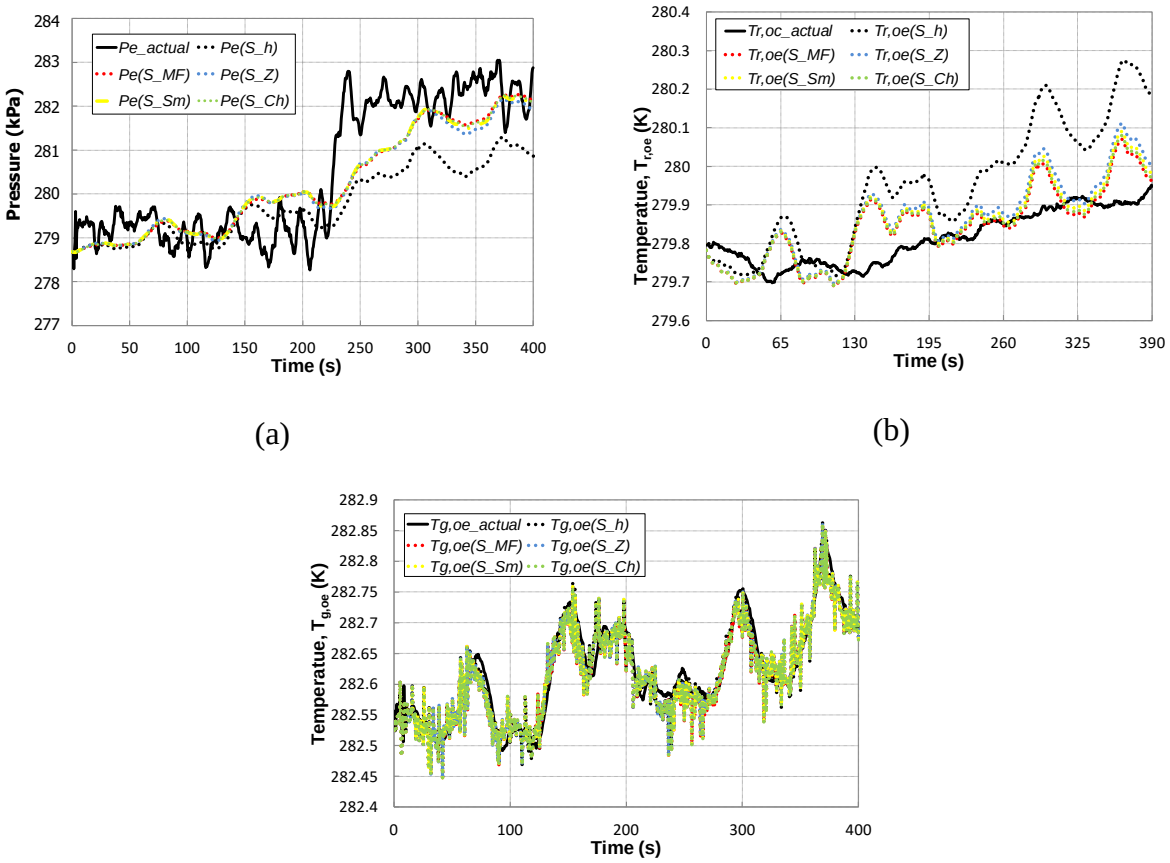

Fig. 5. Test 1. Model outputs due to small decrease in refrigerant mass flux, (a) evaporating pressure, (b) refrigerant outlet temperature, (c) secondary fluid outlet temperature.

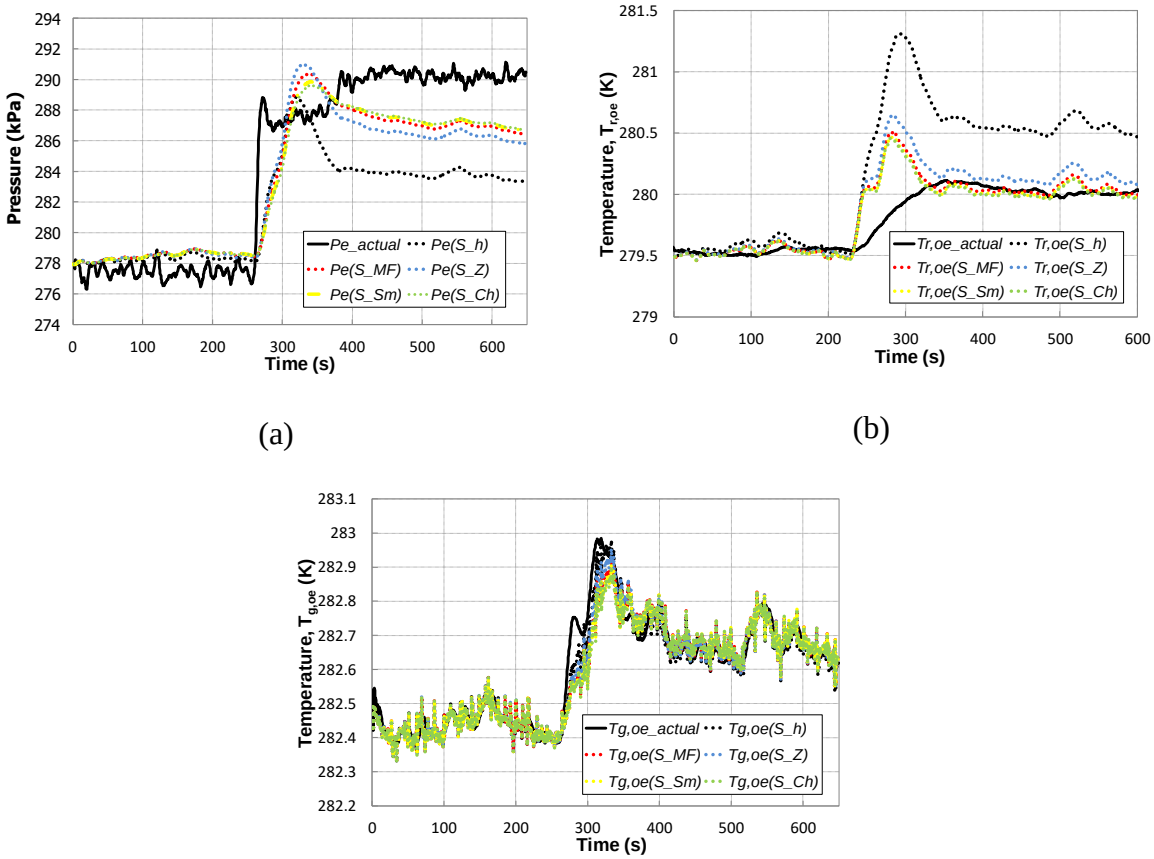

Fig. 6. Test 3. Model outputs due to medium decrease refrigerant in mass flux, (a) evaporating pressure, (b) refrigerant outlet temperature, (c) secondary fluid outlet temperature.

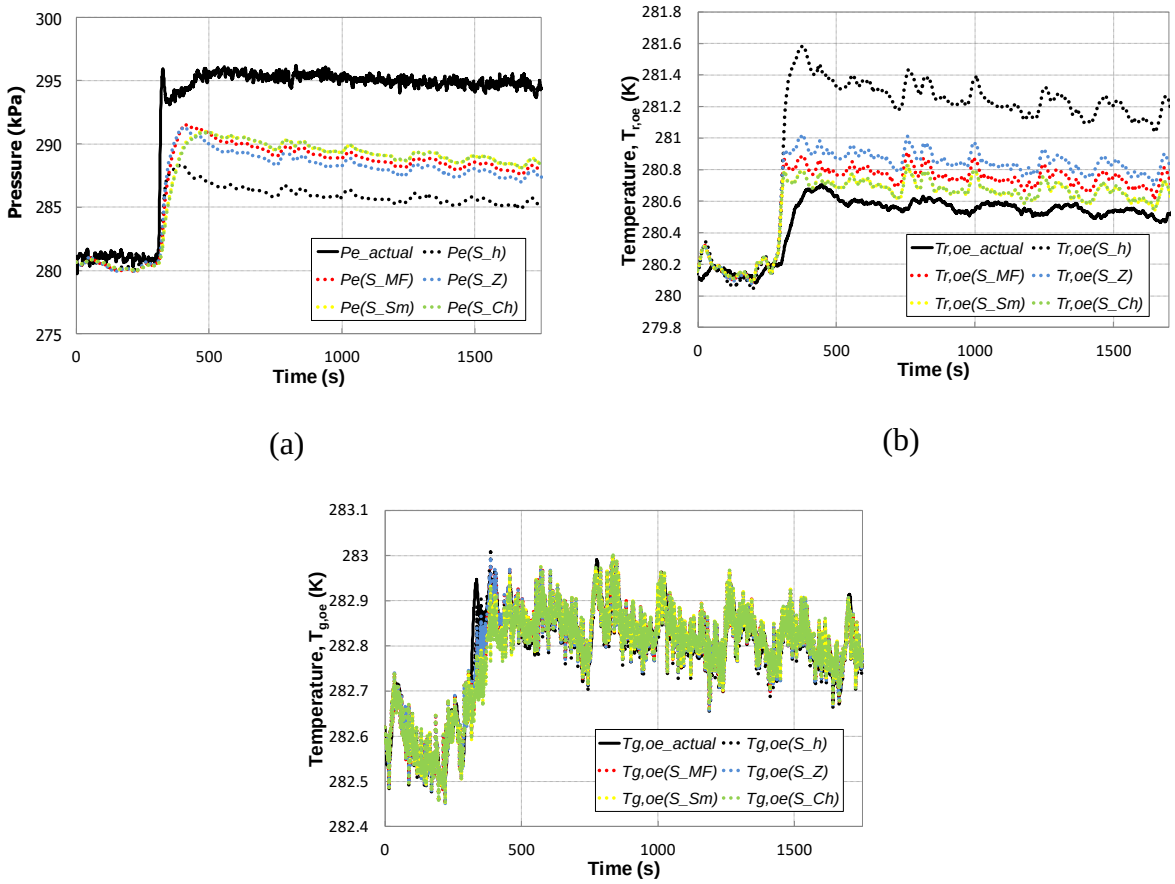

Fig. 7. Test 5. Model outputs due to high decrease in refrigerant mass flux, (a) evaporating pressure, (b) refrigerant outlet temperature, (c) secondary fluid outlet temperature.

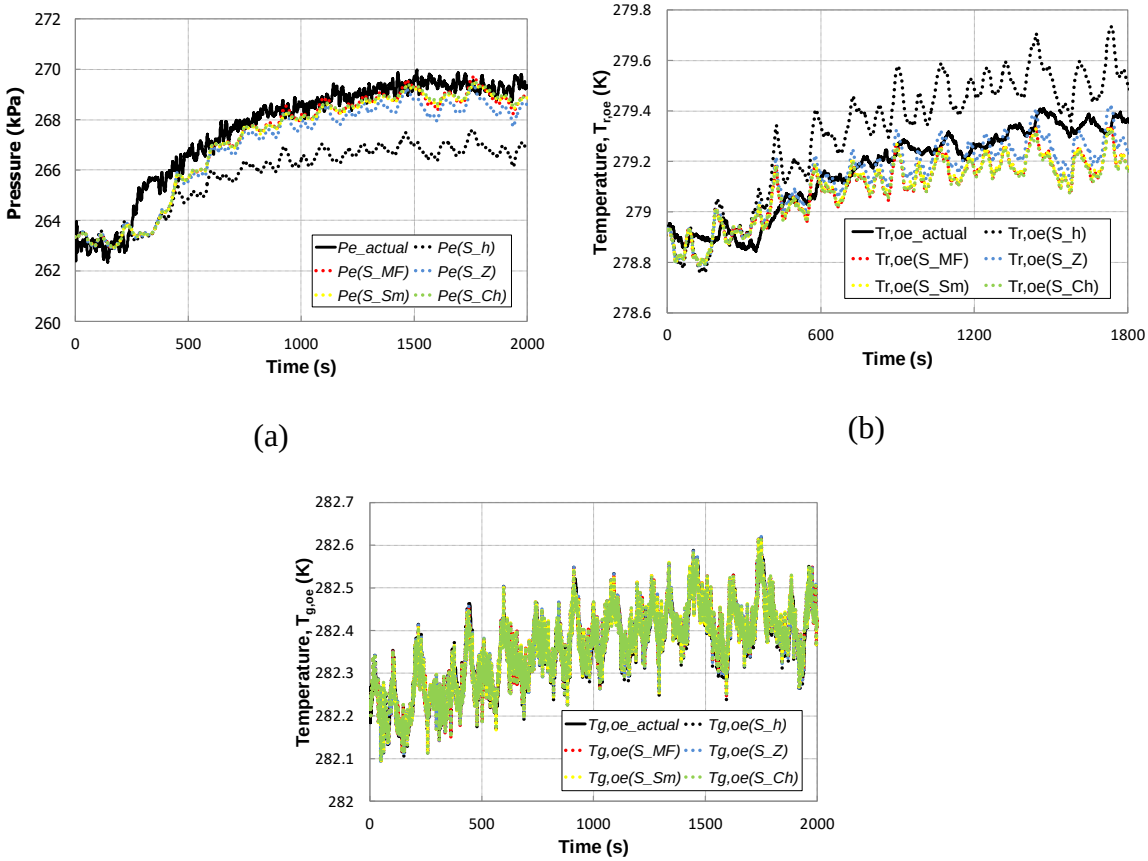

Fig. 8. Test 7. Model outputs due to small decrease in evaporator inlet enthalpy, (a) evaporating pressure, (b) refrigerant outlet temperature, (c) secondary fluid outlet temperature.

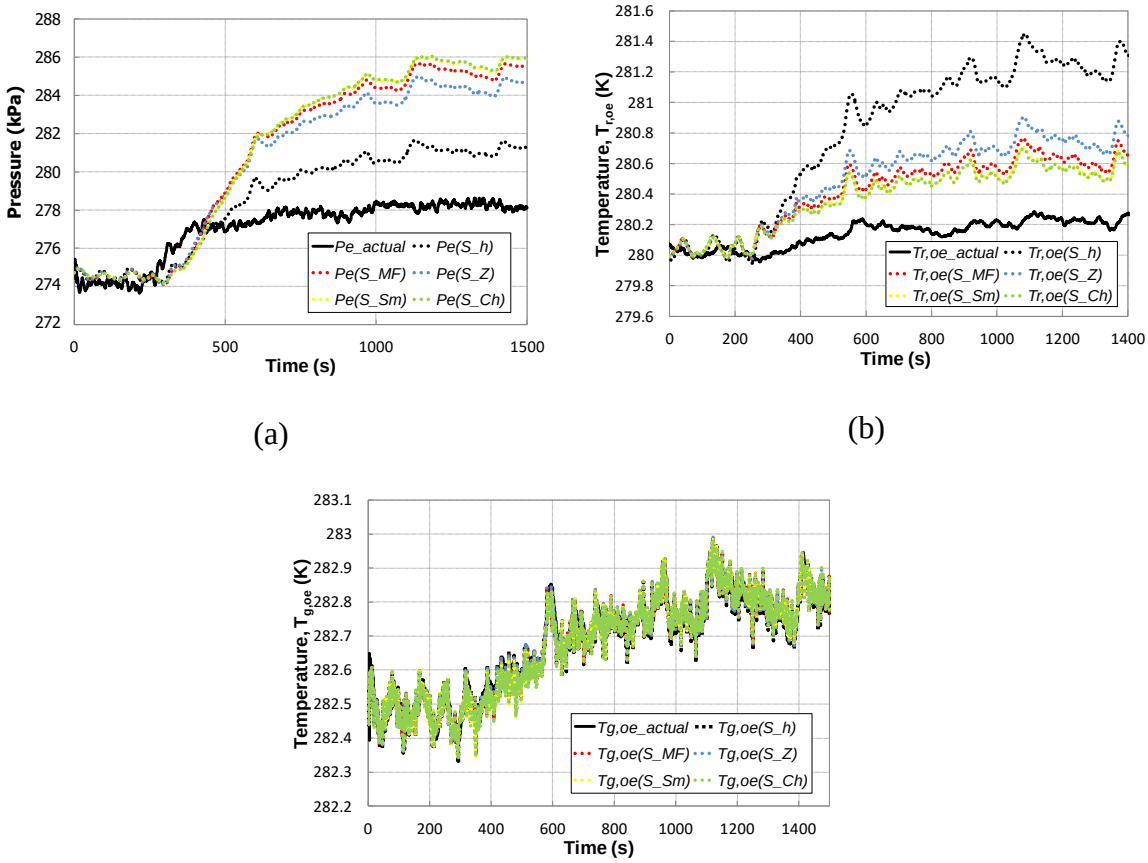

Fig. 9. Test 9. Model outputs due to high decrease in evaporator inlet enthalpy, (a) evaporating pressure, (b) refrigerant outlet temperature, (c) secondary fluid outlet temperature.

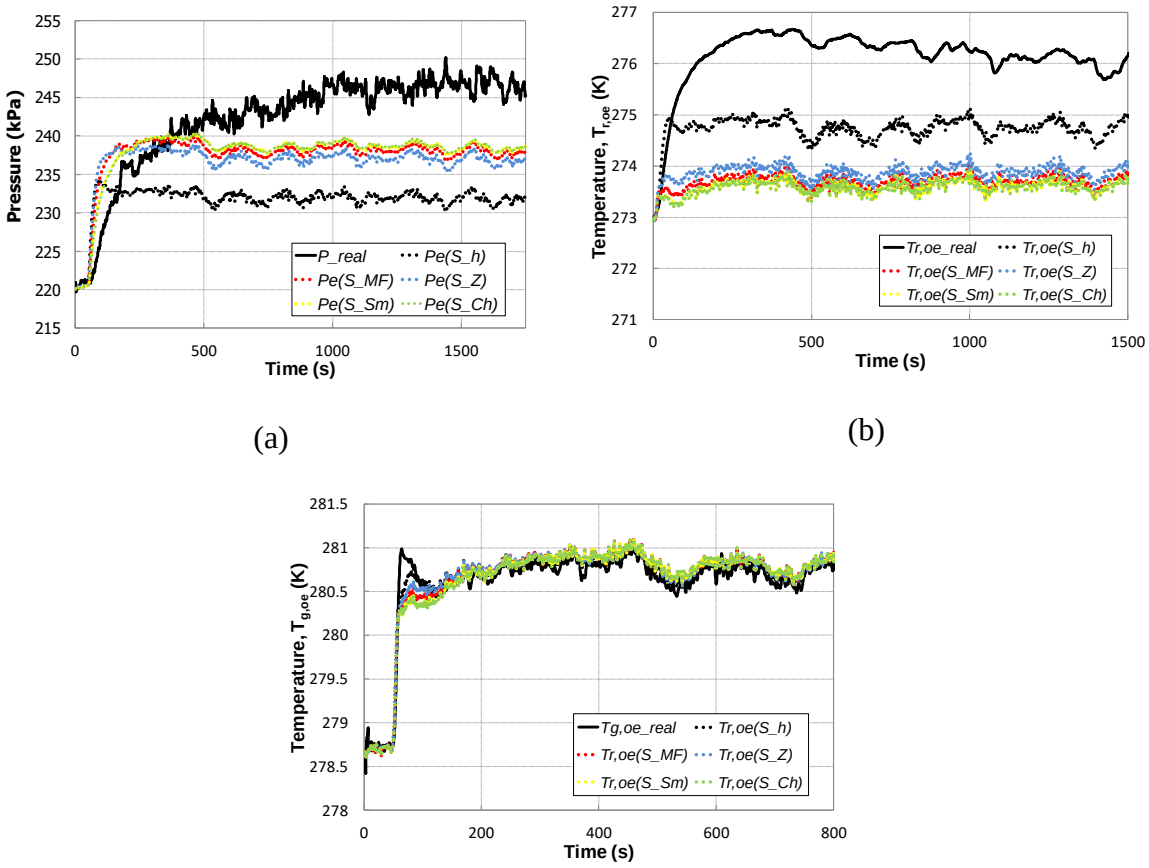

Fig. 10. Test 11. Model outputs due to sharp decrease in evaporator secondary fluid flow, (a) evaporating pressure, (b) refrigerant outlet temperature, (c) secondary fluid outlet temperature.

FIGURE CAPTIONS

Fig. 1. Model scheme.

Fig. 2. Shell-and-tube evaporator inner structure and fluid path (a), and equivalent axial tube with two evaporator zones (b).

Fig. 3. Quality based mean void fraction, S=S_Z.

Fig. 4. Simplified vapour compression plant scheme.

Fig. 5. Test 1. Model outputs due to small decrease in refrigerant mass flux, (a) evaporating pressure, (b) refrigerant outlet temperature, (c) secondary fluid outlet temperature.

Fig. 6. Test 3. Model outputs due to medium decrease in refrigerant mass flux decrease, (a) evaporating pressure, (b) refrigerant outlet temperature, (c) secondary fluid outlet temperature.

Fig. 7. Test 5. Model outputs due to high decrease in refrigerant mass flux decrease, (a) evaporating pressure, (b) refrigerant outlet temperature, (c) secondary fluid outlet temperature.

Fig. 8. Test 7. Model outputs due to small decrease in evaporator inlet enthalpy, (a) evaporating pressure, (b) refrigerant outlet temperature, (c) secondary fluid outlet temperature.

Fig. 9. Test 9. Model outputs due to high decrease in evaporator inlet enthalpy, (a) evaporating pressure, (b) refrigerant outlet temperature, (c) secondary fluid outlet temperature.

Fig. 10. Test 11. Model outputs due to sharp decrease in evaporator secondary fluid flow, (a) evaporating pressure, (b) refrigerant outlet temperature, (c) secondary fluid outlet temperature.

Table 1. Terms z_{ij} in system model.

z_{11}	$A_{cs,e}\rho_L(h_L - h_V)(1-\gamma)$
z_{12}	$\left\{\left[\frac{d(\rho_L h_L)}{dP_e} - \frac{d\rho_L}{dP_e}h_V\right](1-\gamma) + \left[\frac{d(\rho_V h_V)}{dP_e} - \frac{d\rho_V}{dP_e}\right](\gamma) - 1\right\}A_{cs,e}L_{1e}$
z_{21}	$[(\rho_L h_V - \rho_{2e}h_{2e}) + (\rho_V - \rho_L)(\gamma)h_V]A_{sr\_e}$
z_{22}	$\left\{\left[\left(\frac{\partial\rho_{2e}}{\partial P_e}\Big\|_{h_{2e}}\right) + 0.5\left(\frac{\partial\rho_{2e}}{\partial h_{2e}}\Big\|_{P_e}\right)\left(\frac{dh_V}{dP_e}\right)\right]\cdot 0.5(h_o - h_V) + 0.5\rho_{2e}\left(\frac{dh_V}{dP_e}\right) - 1\right\}A_{cs,e}L_{2e}$ $+ \left[\frac{d\rho_L}{dP_e}(1-\gamma) + \frac{d\rho_V}{dP_e}(\gamma)\right]h_V L_{1e}$
z_{23}	$\left[0.5\left(\frac{\partial\rho_{2e}}{\partial h_{2e}}\Big\|_{P_e}\right)\cdot 0.5(h_o - h_V) + 0.5\rho_{2e}\right]A_{cs,e}L_{2e}$
z_{31}	$[(\rho_V - \rho_{2e}) + (\rho_L - \rho_V)\cdot(1-\gamma)]A_{cs,e}$
z_{32}	$\left\{\left[\left(\frac{d\rho_L}{dP_e}\right)(1-\gamma) + \left(\frac{d\rho_V}{dP_e}\right)(\gamma)\right]L_{1e}$ $+ \left[\left(\frac{\partial\rho_{2e}}{\partial P_e}\Big\|_{h_{2e}}\right) + 0.5\left(\frac{\partial\rho_{2e}}{\partial h_{2e}}\Big\|_{P_e}\right)\left(\frac{dh_V}{dP_e}\right)\right]L_{2e}\right\}A_{cs,e}$
z_{33}	$0.5\left(\frac{\partial\rho_{2e}}{\partial h_{2e}}\Big\|_{P_e}\right)A_{cs,e}L_{2e}$
z_{44}	$m_{te}C_{p,t}$
z_{51}	$m_{te}C_{p,t}\left(\frac{T_{t,1e} - T_{t,2e}}{L_{2e}}\right)$
z_{55}	$m_{te}C_{p,t}$

Table 2. Terms y_{ij} in system model.

y_{11}	$\dot{m}_r(h_i - h_V) + \alpha_{in,1e} \cdot A_{in,e}\left(\frac{L_{1e}}{L_{te}}\right)\left(T_{t,1e} - T_{r,1e}\right)$
y_{21}	$\dot{m}_r h_V - \dot{m}_r h_o + \alpha_{in,2e} \cdot A_{in,e}\frac{L_{2e}}{L_{te}}\left(T_{t,2e} - T_{r,2e}\right)$
y_{31}	0
y_{41}	$\alpha_{ex,1e}A_{ex,e}\frac{L_{1e}}{L_{te}}\left(T_{g,1e} - T_{t,1e}\right) - \alpha_{in,1e}A_{in,e}\left(\frac{L_{1e}}{L_{te}}\right)\left(T_{t,1e} - T_{r,1e}\right)$
y_{51}	$\alpha_{ex,2e}A_{ex,e}\frac{L_{2e}}{L_{te}}\left(T_{g,2e} - T_{t,2e}\right) - \alpha_{in,2e}A_{in,e}\frac{L_{2e}}{L_{te}}\left(T_{t,2e} - T_{r,2e}\right)$

Table 3. Equations used to obtain the heat transfer coefficients.

Heat transfer coefficient	Correlation	Equations
Shell side: both regions	Zukauskas (1987)	$\alpha_{ex,(1e,2e)} = \frac{k_g}{D_{ex}} \cdot C \cdot Re_{max}^{m} \cdot Pr_g^{0.36} \cdot \left(\frac{Pr_g}{Pr_{g,t}}\right)^{0.25}$ C and m depends on the configuration and Re_D (Incropera and DeWitt, 1996)
Tube side: evaporating region	Chen (1966)	$\alpha_{in,1e} = sf\alpha_{nb} + F\alpha_{conv}$ $sf = \frac{1}{1 + 0.00000253 Re_{bf}^{1.17}}$ where $Re_{bf} = Re_L \cdot F^{1.25}$ $F = \begin{cases} 1, if\ \frac{1}{X_{tt}} \leq 0.1 \\ 2.35\left(\frac{1}{X_{tt}} + 0.213\right)^{0.736}, if\ \frac{1}{X_{tt}} > 0.1 \end{cases}$ where $X_{tt} = \left(\frac{1-x}{x}\right)^{0.9} \left(\frac{\rho_V}{\rho_L}\right)^{0.5} \left(\frac{u_L}{\mu_V}\right)^{0.1}$ $\alpha_{nb} = 0.00122 \left[\frac{k_L^{0.79} c_{pL}^{0.45} \rho_L^{0.49}}{\sigma^{0.5} u_L^{0.29} h_{LV}^{0.24} \rho_V^{0.24}}\right] \Delta T_{sat}^{0.24} \Delta P_{sat}^{0.75}$ (Forster and Zuber, 1955) $\alpha_{conv} = 0.023 Re_L^{0.8} Pr_L^{0.4} \left(\frac{k_L}{D_{in}}\right)$ (Dittus and Boelter, 1930)
Tube side: superheating region	Gnielinski (1976)	$\alpha_{in,2e} = \frac{k_{r,2e}}{D_{in}} \frac{\left(\frac{f_{2e}}{8}\right)(Re_{2e} - 1000) Pr_{2e}}{1 + 12.7\left(\frac{f_{2e}}{8}\right)^{1/2}\left(Pr_{2e}^{2/3} - 1\right)}$

Table 4. Tube characteristics.

Number	76
D_{in}/D_{ex}	$8.22 \times 10^{-3}/9.52 \times 10^{-3}$ m
Thickness of inner microfins	0.2×10^{-3} m
Total length	0.92 m
External exchange surface	1.81 m^2
Tube-side volume	3.3×10^{-3} m^3
Shell-side volume	8×10^{-3} m^3

Table 5. Measured parameters and equipment uncertainty.

Measured parameters	Sensor	Uncertainty
Temperatures	K-type thermocouples	±0.3 K
Pressures	Piezoelectric pressure transducers	±0.1%
Mass flow rate	Coriolis mass flow meter	±0.22%
Compressor power consumption	Digital wattmeter	±0.5%
Rotation speed	Capacitive sensor	±1%
Volumetric flow rate	Electromagnetic flow meters	±0.33%

Table 6. Changes of parameters that originate the transients.

Test	$\dot{m}_r$ $(kg\ s^{-1})$	$h_{i,avg}(kJ\ kg^{-1})$	$\dot{V}_g(m^3 s^{-1})$	$T_{g,i}$ (K)
Test 1	0.0563→0.0548	256.6(±0.1)	8.2 10^{-4}(±1.4 10^{-6})	285.16(±0.08)
Test 2	0.0555→0.0569	259.7(±0.2)	8.2 10^{-4}(±2.8 10^{-6})	285.09(±0.06)
Test 3	0.0556→0.0503	248.7(±0.9)	8.2 10^{-4}(±2.8 10^{-6})	285.11(±0.07
Test 4	0.0483→0.0543	266.8(±1.5)	8.2 10^{-4}(±1.4 10^{-6})	285.19(±0.05)
Test 5	0.0569→0.0497	257.4(±2.1)	8.2 10^{-4}(±2.8 10^{-6})	285.11(±0.06)
Test 6	0.0497→0.0603	261.0(±3.0)	8.2 10^{-4}(±2.8 10^{-6})	285.08(±0.07)
Test 7	0.0599(±0.0003)	251→258	8.2 10^{-4}(±1.7 10^{-6})	285.10(±0.07)
Test 8	0.0553(±0.0003)	256→251	8.2 10^{-4}(±2.2 10^{-6})	285.14(±0.07)
Test 9	0.0591(±0.0007)	264→273	8.2 10^{-4}(±2.8 10^{-6})	285.15(±0.07)
Test 10	0.0552(±0.0005)	270→260	8.2 10^{-4}(±2.5 10^{-6})	285.14(±0.07)
Test 11	0.0546(±0.0031)	242.0(±1.1)	3.3 10^{-4}→5.6 10^{-4}	284.76(±0.16)
Test 12	0.0489(±0.0030)	234.1(±1.1)	5.6 10^{-4}→3.3 10^{-4}	284.56(±0.21)

Table 7. RMS values.

		S_h	S_{MF}	S_Z	S_{Sm}	S_{Ch}
Test 1	P_e	1273	943	967	951	945
	$T_{r,oe}$	0.1734	0.0772	0.0908	0.0835	0.0799
	$T_{g,oe}$	0.0465	0.0470	0.0467	0.0468	0.0469
Test 2	P_e	918	737	765	759	764
	$T_{r,oe}$	0.0917	0.0734	0.0715	0.0757	0.0758
	$T_{g,oe}$	0.0502	0.0497	0.0501	0.0483	0.0482
Test 3	P_e	4527	2731	3047	2643	2622
	$T_{r,oe}$	0.5365	0.1654	0.2153	0.1553	0.1522
	$T_{g,oe}$	0.0610	0.0724	0.0678	0.0745	0.0754
Test 4	P_e	4339	2273	2657	2121	2124
	$T_{r,oe}$	0.957	0.097	0.158	0.071	0.070
	$T_{g,oe}$	0.048	0.051	0.049	0.055	0.056
Test 5	P_e	8236	5598	6085	5338	5356
	$T_{r,oe}$	0.6396	0.1958	0.2783	0.1305	0.1310
	$T_{g,oe}$	0.0478	0.0509	0.0492	0.0551	0.0554
Test 6	P_e	8106	4114	4818	4065	3939
	$T_{r,oe}$	0.7656	0.1921	0.2219	0.1942	0.1940
	$T_{g,oe}$	0.073	0.093	0.083	0.091	0.094
Test 7	P_e	2105	857	1021	860	838
	$T_{r,oe}$	0.183	0.119	0.087	0.115	0.123
	$T_{g,oe}$	0.0446	0.0448	0.0447	0.0448	0.0448
Test 8	P_e	768	1356	1209	1325	1349
	$T_{r,oe}$	0.2722	0.1112	0.1351	0.1156	0.1115
	$T_{g,oe}$	0.6879	0.5179	0.5499	0.5238	0.5177
Test 9	P_e	2146	5011	4453	5254	5272
	$T_{r,oe}$	0.7908	0.3276	0.4192	0.2821	0.2771
	$T_{g,oe}$	0.0450	0.0447	0.0444	0.0455	0.0457
Test 10	P_e	1299	3813	3297	4069	4082
	$T_{r,oe}$	0.2985	0.1553	0.0858	0.2051	0.2085
	$T_{g,oe}$	0.0432	0.0429	0.0428	0.0431	0.0432
Test 11	P_e	11950	6713	7671	6147	6089
	$T_{r,oe}$	1.3698	2.4007	2.2173	2.4897	2.4976
	$T_{g,oe}$	0.2384	0.2478	0.2451	0.2504	0.2507
Test 12	P_e	15201	13208	13258	13539	13631
	$T_{r,oe}$	2.711	3.381	3.248	3.442	3.451
	$T_{g,oe}$	0.5768	0.5690	0.5725	0.5669	0.5666